# Computational Modeling on Binding Interactions of Cyclodextrin s with the Human Multidrug Resistance P-glycoprotein Toward Efficient Drugdelivery System Applications

Michael González-Durruthy[1,2,*], Riccardo Concu[1,*], Laura F. Osmari Vendrame[3], Mirkos Ortiz Martins[3], Ivana Zanella[3], Juan Manuel Ruso[2] and Maria Natália Dias Soeiro Cordeiro[1,*]

*[1]LAQV-REQUIMTE, Department of Chemistry and Biochemistry, Faculty of Sciences, University of Porto, 4169-007 Porto, Portugal; [2]Soft Matter and Molecular Biophysics Group, Department of Applied Physics, University of Santiago de Compostela, 15782, Santiago de Compostela, Spain; [3]Post-Graduate Program in Nanoscience, Franciscan University (UFN), 97010-032, Santa Maria, RS, Brazil*

**Abstract:** ***Background*:** Herein, molecular docking approaches and DFT *ab initio* simulations were combined for the first time, to study the key interactions of cyclodextrins (CDs: α-CD, β-CD, and γ-CD) family with potential pharmacological relevance and the multidrug resistance P-gp protein toward efficient drug-delivery applications.The treatment of neurological disorders and cancer therapy where the multiple drug-resistance phenomenon mediated by the P-gp protein constitutes the fundamental cause of unsuccessful therapies.

***Objectives*:** To understand more about the CD docking mechanism and the P-gp.

***Methods*:** In order to achieve the main goal, the computational docking process was used. The observe docking-mechanism of the CDs on the P-gp was fundamentally based on hybrid backbone/side-chain hydrophobic interactions, and also hybrid electrostatic/side-chain interactions of the CD-ligands' OH-motifs with acceptor and donor characteristics, which might theoretically cause local perturbations in theTMD/P-gp inter-residues network, influencing ligand extrusion through the blood-brain barrier. P-gp residues were conformationally favored. Despite the structural differences, all the cyclodextrins exhibit very close Gibbs free binding energy values (or affinity) by the P-gp binding site (transmembrane domains - TMDs).

***Result*:** The obtained theoretical docking-mechanism of the CDs on the P-gp was fundamentally based on hybrid backbone/side-chain hydrophobic interactions, and also hybrid electrostatic/side-chain interactions of the OH-motifs of the CD-ligands with acceptor and donor properties which theoretically could induce allosteric local-perturbations in the TMDs-inter-residues network of P-gp modulating to the CD-ligand extrusion from the blood-brain-barrier (or cancer cells).

***Conclusion*:** Finally, these theoretical results open new horizons for evaluating new nanotherapeutic drugs with potential pharmacological relevance for efficient drug-delivery applications and precision nanomedicine.

**Keywords:** Cyclodextrins, P-glycoprotein, *ab initio-DFT*, Molecular docking, Nanomedicine, Computational modeling, Binding interactions, Drug selivery system, Multidrug resistance.

## 1. INTRODUCTION

The pharmacokinetic bioavailability in the central nervous system for a wide diversity of compounds (including nanoparticles) is critically determined by both drug and blood-brain barrier (BBB) properties, where the P-gp protein is embedded [1, 2]. The P-glycoprotein (Pgp), corresponds to a ubiquitous large superfamily of membrane efflux transporters of the ABC superfamily (*i.e.*, ABCB1 transporters), which plays a central role neurological disorders and multiple drug-resistance in cancer, the P-gp has been well-recognized to be a biomarker of overall poor chemotherapy response and prognosis. From the structural point of view, the P-gp is formed by a single polypeptide with a molecular weight of ~170 kDa, organized in two functional units with pseudo-2-fold molecular symmetry, each one comprising six transmembrane α-helices domains

*Address correspondence to these authors at the LAQV-REQUIMTE, Department of Chemistry and Biochemistry, Faculty of Sciences, University of Porto,4169-007 Porto, Portugal; Tel: +351-220402502;
E-mails: michael.durruthy@fc.up.pt (M. González-Durruthy); riccardo.concu@fc.up.pt (R. Concu); ncordeir@fc.up.pt (N.D.S. Cordeiro)

(TMD1, TMD2) and the cytoplasmic nucleotide-binding domain (NBD), linked by a small polypeptidic sequence. From the functional point of view, the P-gp actively participates in the efflux process of a wide range of physiological substrates and potentially toxic drugs and xenobiotics (mainly hydrophobics) out of the cell through an ATP-dependent mechanism being found at the apical surface of the kidney proximal tubule cells, the canalicular membrane of hepatocytes, pancreas, villous intestinal cells, and blood–tissue barriers (*e.g*., brain, placenta, testis).

Currently, an emerging consensus shows that the TMD regions of P-gp protein can modulate its physiological function through different mechanisms as i) blocking efflux-related conformational changes, ii) reducing the drug-stimulated ATPase activity, or iii) affecting the transporter's structural stability to decrease drug efflux ratios [3-7]. Following this idea, some drugs (as Rhodamine B, Verapamil, and Valspodar) have shown significant selectivity by the TMD binding sites of P-gp protein exercising an inhibition response based on "drug-induced fit" mechanism based on a TMD inhibition response [8].

In this regard, it is widely understood that an efficient drug-delivery procedure should address the molecular mechanisms of interaction of a specific drug (*i.e*., CDs) with the relevant binding site of the P-gp to ensure the success of neuropharmacology and chemotherapeutic tactics (*i.e*., TMD regions). In this context, a large number of preclinical studies have experimentally demonstrated that the pharmacological modulation of P-gp can directly affect the optimal concentrations of several substrates in the brain and cancer cells. Nevertheless, computational studies on the interaction mechanisms of P-gp with nanotherapeutic drugs (CDs) are still largely ignored. Thus, the main objective of the present study was to investigate the pharmacodynamic binding interactions of a theoretically modeled cyclodextrins family (α-CD, β-CD, and γ-CD) with the TMDs main cavity belonging to P-gp protein, which is involved in the multi-drug resistance mechanisms during the chemotherapy, and actively participating in the drugs and xenobiotic-extrusion from the blood-brain-barrier modulating or restricting the access of therapeutic drugs to the brain during the therapy of neurological disorders [9-14].

Then, considering the pharmacological relevance of the current problem, we propose for the first time the use of an *in silico* nanopharmacology approach combining molecular docking and "Density Functional Theory" simulations (*i.e*., DFT *ab initio* simulation) to evaluate the structural, electronic, and binding affinity properties of the CDs family interacting with the target P-gp protein [15, 16]. The present study could open new horizons toward an efficient and rational design of new drug-delivery systems for potential nanobiomedical applications.

## 2. MATERIALS AND METHODS

### 2.1. Molecular Docking Simulation

Herein, molecular docking experiments based on Autodock Vina software were performed in order to predict the binding interactions (ΔG docking binding affinity, kcal/mol) between the cyclodextrin family α-CD, β-CD and γ-CD and the P-gp [17]. Firstly, the 3D-protein structure of the human P-gp was theoretically obtained by using the Phyre2 Protein Fold Recognition Server [18] due to the absence of the crystallographic P-gp model.pdb in the *RCSB Protein Data Bank*. For this purpose, the Phyre2 server uses an advanced remote homology modeling detection algorithm to rigorously build a 3D-protein molecular structure as a proper crystallographic pdb.model with high accuracy (> 98%); just by using the NCBI FASTA amino-acid sequence of the human P-gp as input file [18].

Before the docking experiments, the P-gp structure was prepared using the AutoDock Tools 4 and AutoDock Vina software. The P-gp hydrogen atoms were added, according to appropriate hybridization geometry, to those atoms based on built-in modules to add partial charges, protonation states followed by bond orders assignment and set up rotatable bonds of the P-gp like pdb X-ray crystallography-structure [19, 20].

Afterward, the prediction of the P-gp binding sites (*i.e*., site composing the TMD region of the P-gp) was carried out by using DeepSite software, where all the molecular descriptors related to cavities and small tunnels of the protein as van der Waals surface were detected. To perform the simulation experiments, we used one simulation box that determined the potential concave area for the binding of CD-ligands. Herein, the binding pockets detection procedure was performed using the P-gp grid-box size with dimensions of X= 40 Å, Y= 40 Å, Z =40 Å and a center coordinates of X=-24.4Å, Y= 5.1Å, Z = -3.2 Å before to the P-gp interaction evaluation with the ligands under study (*i.e*., α-CD, β-CD and γ-CD).

To do this, the Autodock Vina software applies thermodynamic force field parameters as part of its thermodynamics scoring function, which allows predicting the Gibbs free energy (or binding affinity as FEB values Y $\Delta G_{bind}$ expressed in kcal/mol) from the formed docking complexes (P-gp plus CDs: α-CD, β-CD, γ-CD and rhodamine B used as reference control of maximum theoretical P-gp inhibition). For this instance, the cited docking complexes were considered thermodynamically stable when the obtained ΔG or FEB values < 0 kcal/mol, otherwise categorized like energetically unfavorable, pointing out low or complete absence of binding affinity.

The $\Delta G_{bind}$ values can be expressed as the sum of individual molecular mechanics terms (Amber force-field parameters) for standard-chemical potentials (ΔGbind Y FEB), including the van der Waals interactions ($\Delta G_{vdW}$), hydrogen bond ($\Delta G_{H\text{-}bond}$), electrostatic interactions ($\Delta G_{electrost}$), and intra-molecular ligands interactions ($\Delta G_{int}$) from empirically validated Autodock Vina scoring function according to the general thermodynamic equation **1** depicted below:

$$FEB_{dock} \approx \Delta G_{bind} = \Delta G_{vdW} + \Delta G_{H\text{-}bond} + \Delta G_{electrost} + \Delta G_{int} \quad (1)$$

Furthermore, it is well known that the Autodock Vina scoring function presents an optimal-linear correlation with the individual chemical potentials cited above. Also, it is important to note that overall docking parameters are based on distance-dependent atom-pair interactions ($d_{ij}$) from the CD-ligand$_{(i)}$ and the P-gp protein$_{(j)}$.

Next, the docking complexes between the P-gp and the CDs with the lowest Gibbs docking free energy of binding (FEB negatives value) were obtained. Also, the best root-mean-square-deviation (R.M.S.D) was set as a criterion of docking accuracy for R.M.S.D < 2Å according to equation **2**.

$$\text{R. M. S. D}\left(\text{pose}_{\text{i-CDli}\approx\Delta\text{nd}}, \text{pose}_{\text{-P+p}}\right) = \overline{Q\frac{\sum_{n}(\text{TtoU}_{(\text{iV.X li}\approx\Delta\text{nd})}\text{-TtoU}_{(\text{ZV}[\approx\backslash))}]}{n}} \quad (2)$$

Then, the free energy of binding (ÆGbind Y FEB values; kcal/mol) of the formed docking complexes (*i.e.*, P-gp/CDs: P-gp/α-CD, P-gp/β-CD, and P-gp/γ-CD) were obtained. It is important to note that the Rhodamine B (*i.e.*, the specific inhibitor of the P-gp/TMDs-ligand extrusion binding domains of P-gp) was used as reference control of simulation for comparison purposes for all the simulations.

Next, the 2D/3D-LigPlot interactions diagrams were performed in order to identify key amino acid residues involved in the CDs-interactions (as hydrophobic, hydrogen bond, and electrostatic interactions) with the critical binding site of the P-gp/TMDs [21]. The Lig-Plot algorithm automatically generates schematic 2D/3D diagrams showing details to represent the inter-atomic interactions for all the docking complexes (*i.e.*, P-gp/CDs: P-gp/α-CD, P-gp/β-CD, and P-gp/γ-CD) at molecular and atomistic-level [21].

In order to ensure the accuracy of the molecular docking calculations, several runs started from random conformations of the ligands (CDs: P-gp/α-CD, P-gp/β-CD, and P-gp/γ-CD) were performed. For this instance, the exhaustiveness parameter was set at 50 (*i.e.*, the number of CDs binding conformations in the P-gp binding site which is placed in the transmembrane domain (TMDs) of the P-gp protein) [19-22].

### 2.2. Local Perturbation Response Analysis

This computational algorithm evaluates the degree of perturbation induced by a given ligand (*i.e.*, CDs: α-CD, β-CD and γ-CD) in the target residues network of a given receptor (*i.e.*, P-gp/TMDs protein) based on elastic normal mode analysis. Herein, the allosteric local perturbations in the P-gp/TMDs were determined by measuring the P-gp/TMDs binding-residue displacements from their equilibrium positions for both, i) unperturbed (*i.e.*, P-gp/TMD unbound state) and ii) the perturbed state (*i.e.*, P-gp/TMDs bound state, in the presence of CDs ligands), see equation (3):

$$e_{p_{(i)}} = \frac{1}{N_{\Delta}} \sum^{N_{\Delta}}_{=1} \text{jp} - \text{u j} \quad (3)$$

Where, $e_{p(i)}$ represents the effect of the allosteric local perturbation in the normal elastic mode (*i*), the term $p_j$ is the displacement of the P-gp/TMDs residue (*j*) in the perturbed normal mode (under CD-ligand interaction), and the term $u_j$ represents the displacement of an individual P-gp/TMD residue (*j*) in the unperturbed mode (or equilibrium position), and N*a* is the number of interacting residues identified in the 2D/3D-lig-plot approach [23-25].

### 2.3. Density Functional Theory

The energetic, structural, and electronic properties of the P-gp/TMD residues under interaction with CDs were simulated using DFT *ab initio* calculations [26]. For this purpose, the SIESTA code was used, which performs full self-consistent calculations by solving the Kohn–Sham equations and using numerical atomic orbitals as basis sets [27, 28]. Here, for overall interactions, a grid integration cutoff of 200 Ry was used to represent the charge density. Besides, the atomic structures were relaxed until the residual forces were less than 0.05 eV/Å for all atoms in the structures of P-gp/TMDs and residues and CD-ligands. The interactions between the core and the valence electrons were described by improved Troullier – Martins pseudopotentials [29], whereas the molecular orbitals were making use of a localized double zeta plus polarization (DZP) basis set.

Next, the correlation energies based on the local density approximation (LDA) were set, as proposed by Perdew and Zunger [30]. In fact, the LDA approach has been shown to be more suitable than the generalized gradient approximation (GGA) to study weakly interacting systems like the involved in the present work, where the π-π stacking interactions are predominant. The binding energy was calculated using the base overlap error correction (BSSE) [31, 32], according to equation **4**.

$$\text{Ee} = \text{fE(gD} + \text{hip)} - \text{E,gD} + \text{hip}_{+\text{kost}}\text{l} - \text{E(gDi}h\text{osn} + \text{hip)o} \quad (4)$$

where, $E_b$ is the total energy of the system and E (CD + P-gp) is the total energy of an individual CD-ligand plus the different target-residues involved in the docking interactions with P-gp/TMDs. The subscript ‘‘ghost” corresponds to the additional basis wave functions centered at the position of the CDs or at P-gp/TMDs, but without any atomic potential. The values for the minimum distances (Å) between the systems were obtained from the nearest interacting atoms. In this concern, it is important to note that, even if density functional tight-binding (DFTB) could be applied as a good control simulation experiment to enrich our DFT results we strongly suggest that the DFTB method would not introduce statistically significant differences with respect to method DFT *ab initio* simulation proposed in this study from the thermodynamics point of view being the main energetic contributions provided by the previous molecular docking simulations for this instance. This type of methodology has been used in other studies within our research group [31, 32].

## 3. RESULTS

### 3.1. Theoretical Modeling and Preparation of the Cyclodextrin Molecules

Initially, the isolated CDs molecules (α-CD, β-CD and γ-CD) were analyzed, Figs. (**1a-c**); respectively. Then, the

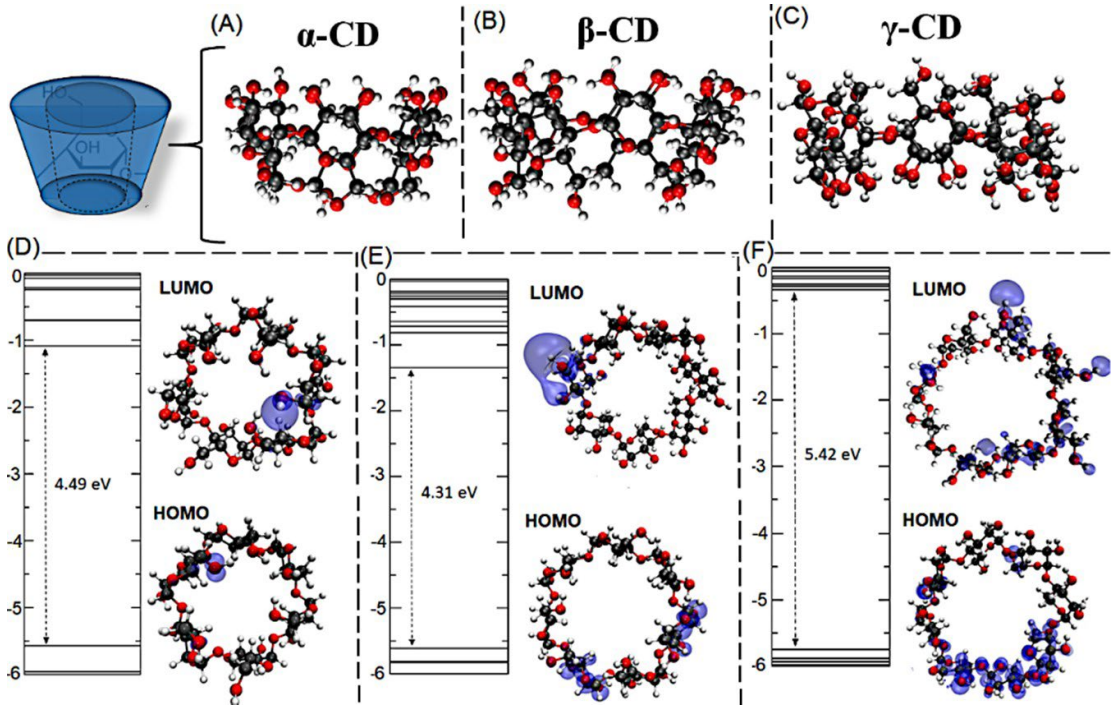


**Fig. (1).** In the top, representation of the optimized structure of the evaluated cyclodextrin family as: (**A**) α-CD (**B**) β-CD, and (**C**) γ-CD. At the bottom, graphical representation of the energy levels with the corresponding plots of electronic charge density obtained ($3.30\times10^{-3}$ e/Å$^3$ isosurface) obtained from the HOMO and LUMO orbitals for the CDs as: (**D**) α-CD, (**E**) β-CD, and (**F**) γ-CD. (*A higher resolution / colour version of this figure is available in the electronic copy of the article*).

electronic levels of the isolated CD molecules, their optimized structures, and the local density of states (LDOS) plot corresponding to the highest occupied molecular orbital (HOMO), and the lowest unoccupied molecular orbital (LUMO) were represented in the Figs. (**1d-f**) for the α-CD, β-CD and γ-CD; respectively. Besides, the energy levels as HOMO-LUMO-differences (ΔH-L) for α-CD, β-CD and γ-CD with the corresponding values of 4.49 eV, 4.31 eV, and 5.42 eV; respectively, were obtained.

For all α-CD, β-CD and γ-CD, was observed that the contribution to the formation of the HOMO was concentrated over the hydroxyl groups with the largest contribution to the oxygen atoms, while the LUMO was mainly located in the hydrogen CD-atoms [32-34].

### 3.2. Computational Modeling and Crystallographic Validation of the Human P-gp

Next, the prediction/identification of the human P-gp/TMD binding sites was carried out as one of the most important step in the macromolecular simulations. To do this, an appropriate crystallographic structural validation of the P-gp protein was performed. Then several modeling procedures for detecting the relevant protein cavities as concave surface within relevant TMDs regions were implemented. In our computational study, the prediction of P-gp/TMDs binding-sites was carried out by applying a machine learning method-based on 3D-Deep Convolutional Neural Networks which identify concave van der Waals regions while excluding convex ones in the P-gp/TMDs protein region evaluated [35]. The obtained results on the structure prediction, identification, and crystallographic validation of P-gp/TMDs binding sites are depicted in Fig. (**2**).

## 4. DISCUSSION

### 4.1. Mechanistic Interpretation of Molecular Docking Results

Molecular docking is one of the most used structure-based methods in rational drug design and molecular recognition, especially when the crystallographic 3D structure of the ligand and relevant target protein are available. The molecular docking simulation has been efficiently extrapolated to traditional *in silico* pharmacology to the newest field of Computational Nanopharmacology toward potential nano-therapeutic drug discovery. In the present study, the computational modeling of the binding interaction of a cyclodextrins family (α-CD, β-CD and γ-CD) with the P-gp protein was carried out for the first time performing a molecular docking.

For this purpose, in order to avoid obtaining false positives from the docking experiment was verified that the modeled residues belonging to the human P-gp.pdb x-ray structure were conformationally favored by considering all their possible conformations within the P-gp protein, which were well-defined by the favored torsion dihedral angles Ψ (Psi) *vs*. Φ (Phi) around the C(α) of the peptide-bond of the P-gp residues in Ramachandran plot [36]. For this instance, conformationally favored dihedral angles Ψ (Psi) *vs*. Φ (Phi) of the P-gp residue were found within the purple contour lines of the Ramachandran plot. Otherwise, they were considered as conformationally-disallowed residues for the

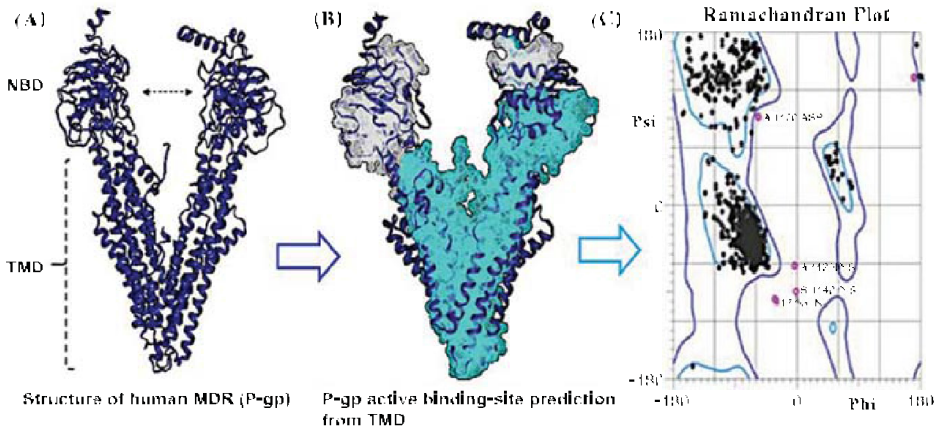


**Fig. (2). (A)** Representation of the whole 3D X-ray crystallographic molecular structure model from human multi-drugs resistance protein transport (P-gp) with the relevant functional domains like P-gp nucleotide-binding domains (NBDs) and the transmembrane domains (TMDs) in outward-facing conformation for CD ligand-extrusion. **(B)** DeepSite prediction of topological cavities of P-gp highlighting the ligand-extrusion binding site (*i.e.*, TMDs as light blue-labelled region). **(C)** Crystallographic validation is based on Ramachandran plot (Phi *vs.* Psi torsion dihedral angles) and the corresponding spatial distribution of Ramachandran outliers (empty pink-labelled circles) outsite of the purple contour line. All the possible combinations of torsion dihedral angles of each P-gp res are depicted by the black dots inside the purple contour line for conformationally-favored P-gp/TMD residues. (*A higher resolution / colour version of this figure is available in the electronic copy of the article*).

**Table 1. Results of binding free energies for the obtained docking complexes for the best CDs/P-gp complexes based on the affinity in kcal/mol. Here, the docking simulation of the Rhodamine B molecule was used as a reference control.**

| Ligands | FEB (kcal/mol) | R.M.S.D (Å) |
|---|---|---|
| Rhodamine B (control) | -8.1 | 1.14 |
| α-CD | -5.1 | 1.97 |
| β-CD | -5.1 | 0.82 |
| γ-CD | -4.0 | 1.70 |

dihedral angles Ψ (Psi) *vs.* Φ (Phi) placed outside of the Ramachandran purple contour line (Ramachandran outliers) [37], (Please refer to Fig. **2C**). Then, it should be pointed out that the aforementioned Ramachandran outliers were not identified for the key binding P-gp/TMD residues involved in the docking interactions with the CDs evaluated.

Following this modeling protocol, the thermodynamics interactions of α-CD, β-CD and γ-CD ligands with P-gp (PDB ID: 4KSB) were evaluated. Then, the obtained Gibbs free energy of binding (FEB, in kcal/mol) showed that all the tested ligands (*i.e.*, α-CD, β-CD, γ-CD, and the Rhodamine B used as reference control) were able to spontaneously interact with P-gp protein with an expected negative FEB value and good crystallographic adjustment based on (R.M.S.D < 2 Å) obtained for three P-gp/CD complexes (P-gp/α-CD, P-gp/β-CD, and P-gp/γ-CD). These theoretical evidence suggest that the three CDs evaluated could mimic the pharmaco-toxicodynamic behavior of the Rhodamine B (*i.e.*, specific P-gp-TMD inhibitor, which represents a measure of the maximum inhibition-based affinity) being used here as reference control of all our simulations in terms of the strength of interactions. See Table **1**.

It is well-known that the P-gp activity increases the membrane permeability for ions associated with changes in the ATP-intracellular levels, which are the source of energy for the P-gp physiological function like the drug extrusion from the blood-brain-barrier [38].

This criterion must be considered as very important due to from the pharmacotoxicodynamic point of view, the cyclodextrin ligands (CDs) could theoretically mimic the molecular mechanisms of interaction of the Rhodamine B in the TMD domain of P-gp in order to ensure the desired selectivity of the CDs ligands (α-CD, β-CD, and γ-CD) toward efficient drug-delivery applications.

In this context, to avoid obtaining false positives on docking interaction results the absence of restricted flexibility for each P-gp_res obtained from the lig-plot analysis was performed. In order to check this, the crystallographic validation based on the Ramachandran plot of Ψ (Psi) *vs*. Φ (Phi) for each ligand-interacting P-gp residue was performed [36]. In this regard, the presence of Ramachandran outliers involved TMD binding residues was not identified in the P-gp whole structure (refer to Fig. **2C**).

Next, the best binding pose obtained for the three CDs studied and the corresponding theoretical control-based Rhodamine B was represented by means of the 2D/3D ezLigPlot diagrams in each simulation experiment [21], as shown in Fig. (**3**) (Rhodamine B), Fig. (**4**) (γ-CD), Fig. (**5**) (α-CD), and Fig. (**6**) (β-CD).

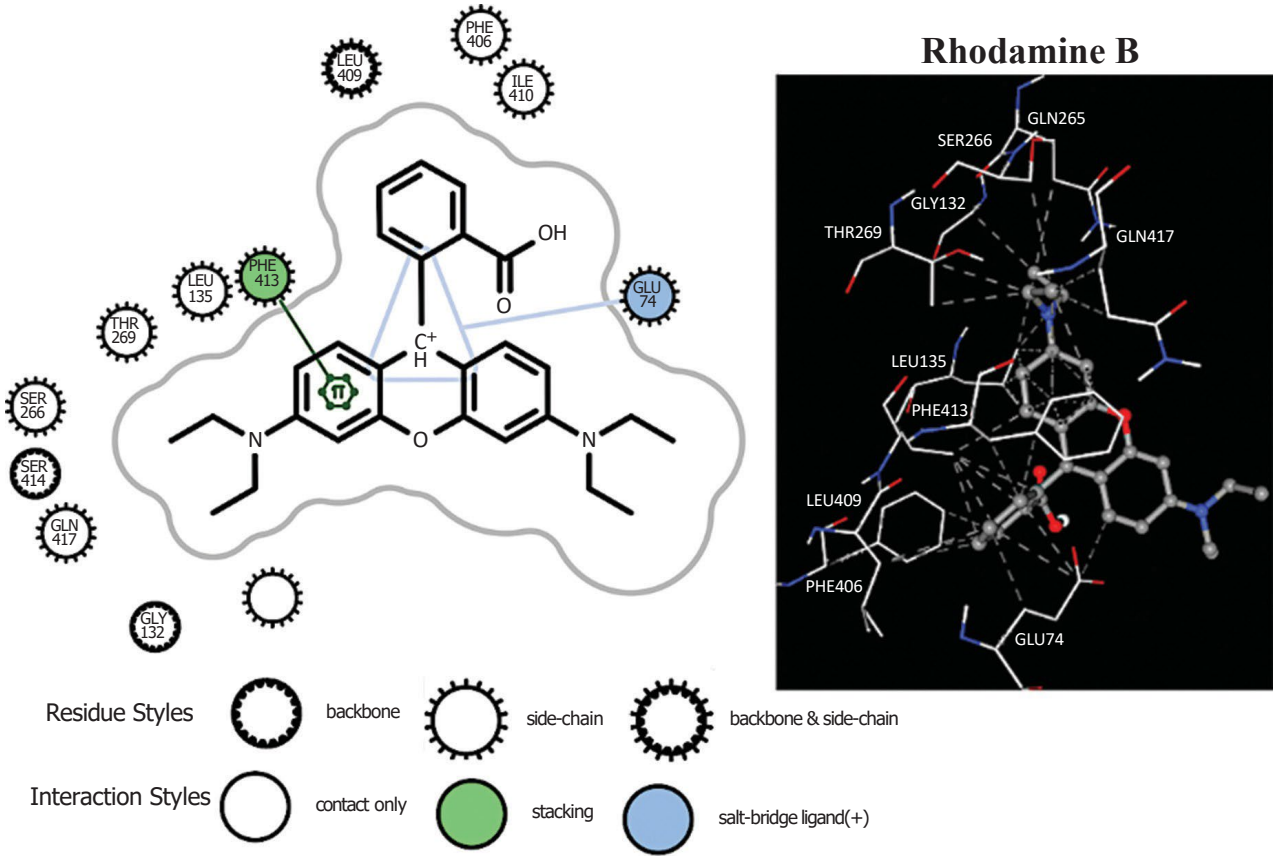


**Fig. (3).** Representation of the 2D/3D lig-plot diagrams for the best docking pose obtained for the Rhodamine B/P-gp complex. (*A higher resolution / colour version of this figure is available in the electronic copy of the article*).

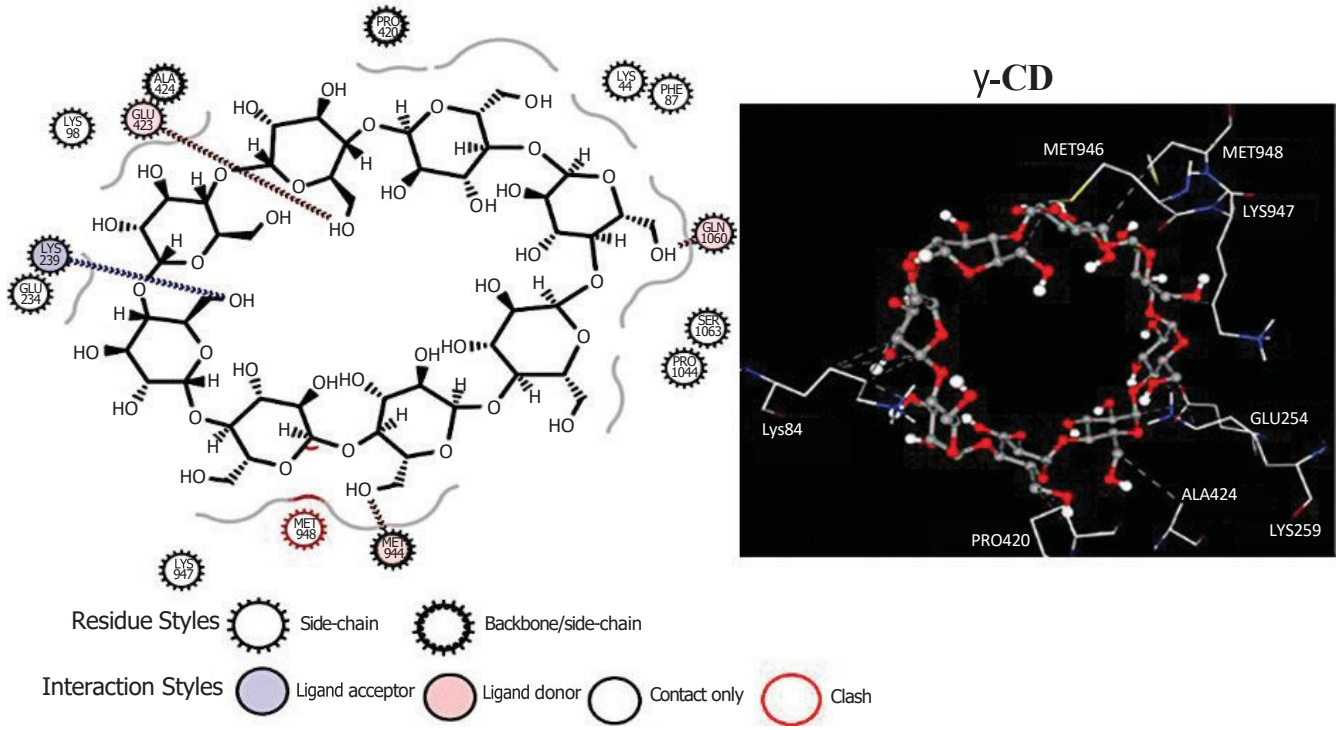


**Fig. (4).** Representation of the 2D/3D lig-plot diagrams for the best docking pose obtained for the docking complex γ-CD/P-gp. (*A higher resolution / colour version of this figure is available in the electronic copy of the article*).

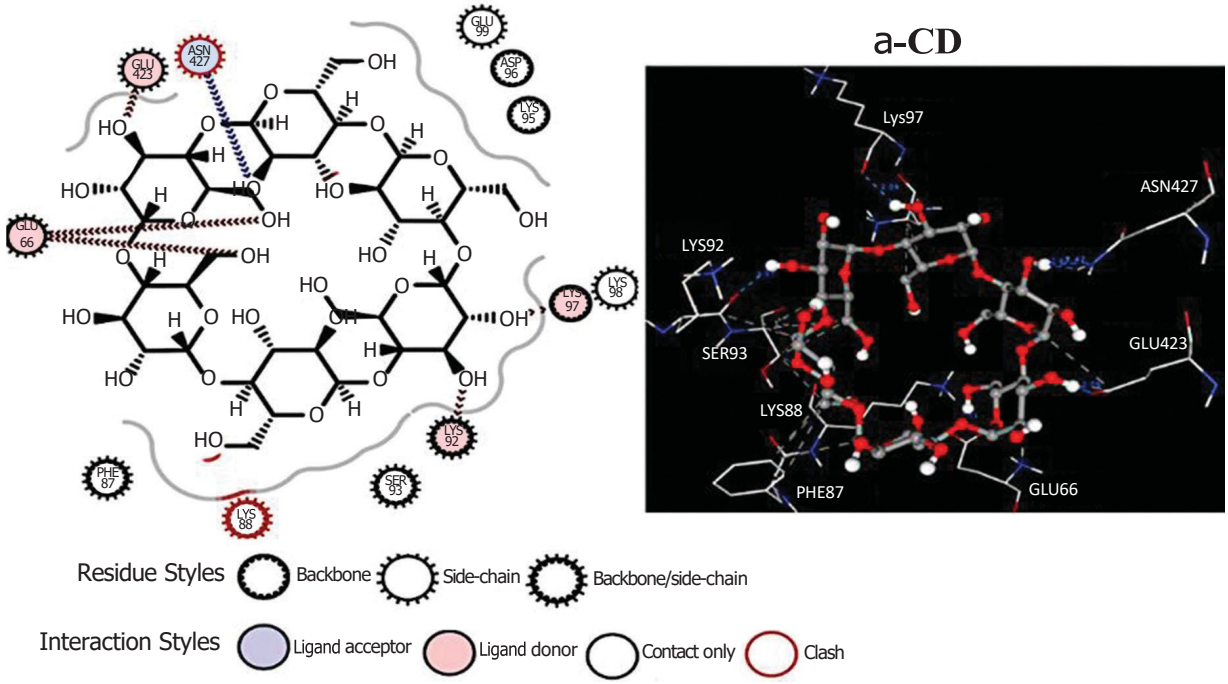


**Fig. (5).** Representation of the 2D/3D lig-plot diagrams for the best docking pose obtained for the docking complex α-CD/P-gp. (*A higher resolution / colour version of this figure is available in the electronic copy of the article*).

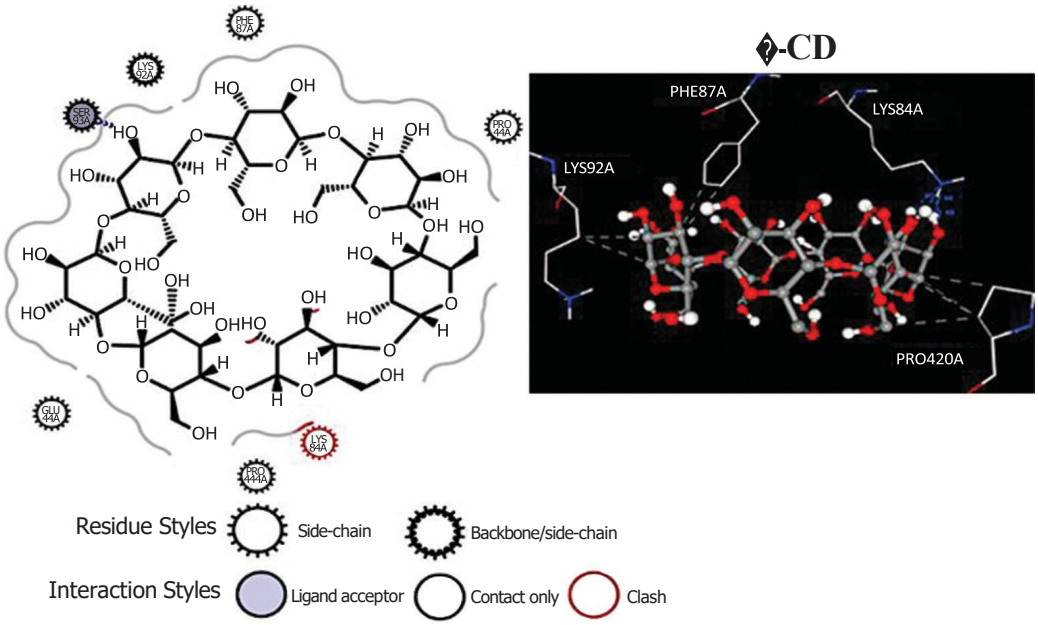


**Fig. (6).** Representation of the 2D/3D lig-plot diagrams for the best docking pose obtained for the docking complex β-CD/P-gp. (*A higher resolution / colour version of this figure is available in the electronic copy of the article*).

The computational results show a prevalence of non-covalent interactions as twelve hydrophobic interactions based backbone & side-chains interactions. Additionally, it was identified a hybrid interaction based on hydrophobic backbone & side-chain interaction with a π-π stacking interaction between the benzene ring of the Rhodamine B with the residue Phe143 and a salt-bridge hydrogen-bond interaction between the central C-H atom of the Rhodamine B with the residue Glu74 forming a triangle-shape. Following this procedure, for the case of the γ-CD, the P-gp docking interactions were mainly based on hydrophobic interactions with the presence of three well-defined electrostatic interactions with a with different toxicodynamic behavior from the biochemical point of view, see Fig. (**4**).

Also, we show a prevalence of non-covalent interactions as hydrophobics contacts mainly based on side-chain and hybrid backbone/side-chain interactions. Besides, four well-defined electrostatic interactions of γ-CD with key P-gp/ TMD residues were identified composed of a ligand-acceptor OH-γ-CD interaction with Lys259, and three OH-

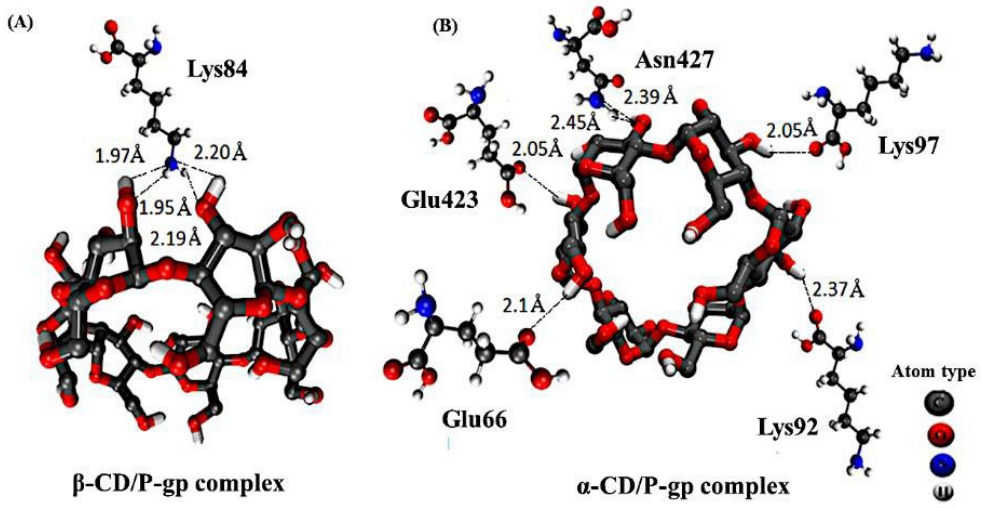


**Fig. (7).** Representation of the refined DFT interaction study for the two-best ranked cyclodextins (β-CD and α-CD) with key target residues of P-gp and considering the critical distance with P-gp residues/TMDs as **(A)** the β-CD interacting with Lys 84 of P-gp/TMDs, and **(B)** α-CD interacting with the target-residues of P-gp as: Asn427, Lys92 (or Lys97), and Glu66(or Glu423) obtained from the previous lig-plot interaction study. The position of the P-gp target-residues with β-CD and α-CD correspond to the exact positions obtained for final crystallographic docking poses. (*A higher resolution / colour version of this figure is available in the electronic copy of the article*).

γ-CD ligand-donor interactions were detected from the key P-gp residues (Glu 423, Met 946, and Gln1060). Next, the docking complex formed between the α-CD and the P-gp was obtained, as represented in Fig. (**5**).

Herein, the α-CD/P-gp complex was mainly formed by the presence of non-covalent hydrophobic side-chain interactions (*i.e.*, Glu99, Lys98, Lys92, Ser93, Lys88, Phe87, Glu66, Glu423, Asn427), and backbone contacts (Lys97, Lys95). By the other hand, the presence of hybrid interactions based on side-chain and electrostatic-based ligand-acceptor (Asn427) and ligand-donor (Lys92, Lys97, and Glu66) were detected as relevant for the stabilization of the docking complex α-CD/P-gp.

Following the order, the lig-plot diagram for the complex β-CD/P-gp was determined, as depicted in Fig. (**6**).

Herein, the docking-mechanism of β-CD was fundamentally based on a hybrid backbone/side-chain hydrophobic interactions (Lys92, Ser93), five hydrophobic side-chain interactions (Phe87, Pro66, Lys84, Pro420, Glu66), and one hybrid electrostatic/backbone/side-chain interactions with the OH-ligand acceptor/donor group of the β-CD with the allosteric regulatory residue of P-gp (Ser93).

### 4.2. Refined DFT Interactions Modeling of CD Ligands with Relevant P-gp Residues

Next, we present refined DFT results by considering the two-best ranked cyclodextins (β-CD and α-CD) with a similar value of free energy of binding of -5.1 kcal/mol (please, refer to Table **1**). The results are presented in Fig. (**7**) as follows.

By the other hand, the inter-atomic hydrogen-bond interaction distances from the CD-ligands (*i.e.*, CD-atom acceptors and CD-atom donors) interacting with the relevant atoms of the P-gp target residues (Lys84, Lys97, Lys92, Glu423, Glu66, Asn427) were calculated by the refined DFT approach from the obtained docking complexes (*i.e.*, β-CD/P-gp, α-CD/P-gp), see Table **2**.

Energy levels for the respective P-gp and β-CD are shown in Fig. (**8**); in addition with the calculated total charge density isosurface plots. Here, the reduction occurs because P-gp target-residues levels are introduced between the HOMO-LUMO gap of the isolated CDs.

In the case of the β-CD interacting with P-gp target-residues, the ΔRHL, independently of the conformation, is reduced by roughly 0.9 %. As can be seen, by the charges localized just in the β-CD and the P-gp target-residues, with no charge lines between the interacting systems (β-CD/P-gp), see Fig. (**8**).

By the other hand, for the α-CD ligand interacting with corresponding target residues of P-gp, the DFT parameter of ΔRHL is independent of the conformation. As depicted in Fig. (**9**), the charges were localized just in the α-CD and the P-gp target-residues, with no charge lines between the interacting DFT systems (*i.e.*, α-CD+P-gp considering the target residues).

Considering the electronic properties of the CDs and the interacting residues of P-gp reported in Table **2**, we strongly suggest that these CDs-ligand are able to interact with good binding affinity based on physical adsorption, these theoretical evidences fits well with the previous molecular docking results. It is important to note that these computational results have extraordinary relevance. Because theoretically indicate that the electronic properties of the cited CDs were not significantly altered by the interaction with P-gp target-residues (Lys84, Lys97, Lys92, Glu423, Glu66, Asn427), suggesting that these privileged ligands (CDs: α-CD and β-CD) could be used as an efficient matrices for efficient drug-delivery applications for potential nano biomedical applications.

**Table 2. Results of the refined DFT parameters as i) inter-atomic bond distances between interacting atoms of key P-gp residues and CD-ligand atoms, ii) binding energy ($E_{bind}$), iii) ΔHL, and iv) the reduction in the HOMO-LUMO gap (ΔRHL) obtained for α-CD and β-CD; just considering the P-gp target-residues forming hydrogen bond contacts in the docking complex with P-gp.**

| Complex | Distance (Å) | $E_{bind}$ (eV) | ΔHL(eV) | ΔRHL(%) |
|---|---|---|---|---|
| β-CD/P-gp | 1.97 ($N_{Lys84}$ - $H_{β-CD}$)<br>2.20 ($N_{Lys84}$ - $H_{β-CD}$)<br>1.95 ($H_{Lys84}$ - $H_{β-CD}$)<br>2.19 ($H_{Lys84}$ - $H_{β-CD}$) | 0,52 | 3.66 | 18.5 |
| α-CD/P-gp | 2.05 ($O_{Lys97}$ - $H_{α-CD}$)<br>2.37 ($O_{Lys92}$ - $H_{α-CD}$)<br>2.05 ($O_{Glu423}$ - $H_{α-CD}$)<br>2.1 ($O_{Glu66}$ - $H_{α-CD}$)<br>2.45 ($N_{Asn427}$ - $H_{α-CD}$)<br>2.39 ($H_{Asn427}$ - $H_{α-CD}$) | 0,31 | 4.24 | 0.9 |

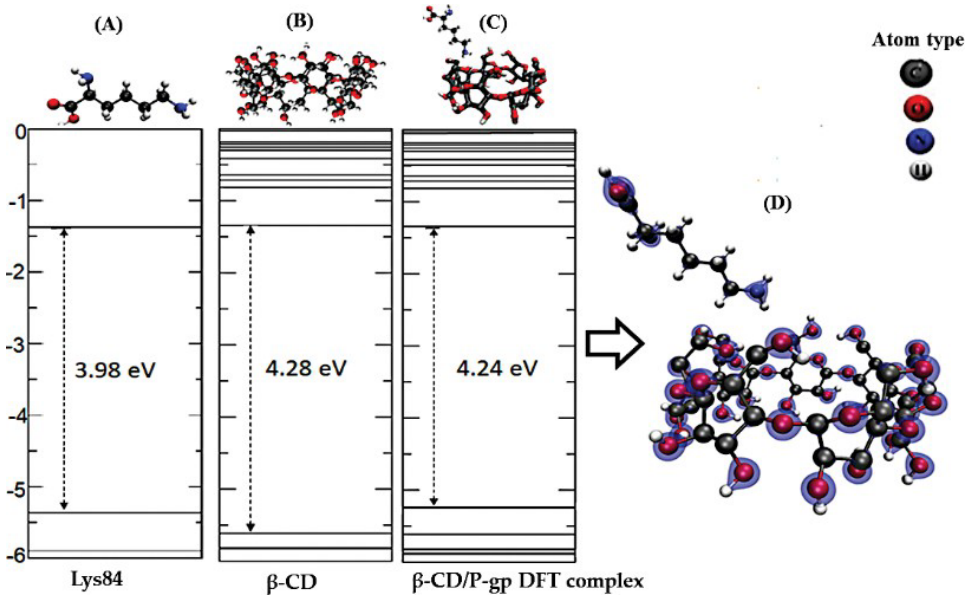


**Fig. (8).** Representation of the electronic levels for the isolated components as **(A)** Lys, **(B)** β-CD; and the component under interaction represented by **(C)** β-CD plus Lys-P-gp. In **(D)** is depicted the total charge density isosurface, for the obtained DFT complex β -CD plus Lys-P-gp by using an orbital charge density isosurfaces 0.0028 e-/(Å)$^3$. (*A higher resolution / colour version of this figure is available in the electronic copy of the article*).

### 4.3. Local Perturbation Response Scanning (LPRS maps)

This approach allowed us to evaluate allosteric local perturbations induced by the ligands (α-CD, β-CD and γ-CD) in the transmembrane domains (TMDs) of the P-gp binding site, as well as, the different amplitude of perturbations (*i.e.*, binding interactions) induced in the inter-residue communication network of the P-gp protein. Because, the transitions across the different functional states from inward to TMDs facing outward during the ligand-extrusion is facilitated and also is dependent, on the TMDs flexibility properties which are directly associated to the allosteric biophysical control that takes place in the inter-residue communication network of the P-gp from both, the unbound and bound state (in the presence of α-CD, β-CD and γ-CD). Herein, the LPRS maps based on elastic network models (ANM) were used to calculate the effectiveness and sensitivity of the propagation of the allosteric signal in the network of binding residues of P-gp, see Fig. (**10**).

According to the simulated LPRS maps (Fig. **10**, **C**-**E**, and **E**) obtained from the docking complexes (γ-CD/ P-gp, α-CD/ P-gp, and β-CD/ P-gp); we strongly suggest that the CDs studied exhibit a significant difference in the pattern of interaction compared with the docking complexes used as simulation controls (Figs. **10 A** and **B**) (unbound or unperturbed P-gp/TMD binding-site, and the Rhodamine B/ P-gp. Herein, we use the ANM models by using rotation-translations blocks approximation (RTB model) to investigate the collective fluctuations (or motions) in the low-frequency normal modes of the P-gp protein. Where, the target TMD residues of P-gp are split into n-(b)-blocks formed by one or of a few consecutive TMD-binding residues that belong to the different polypeptides of the TMD-chains which could potentially bind with the CDs

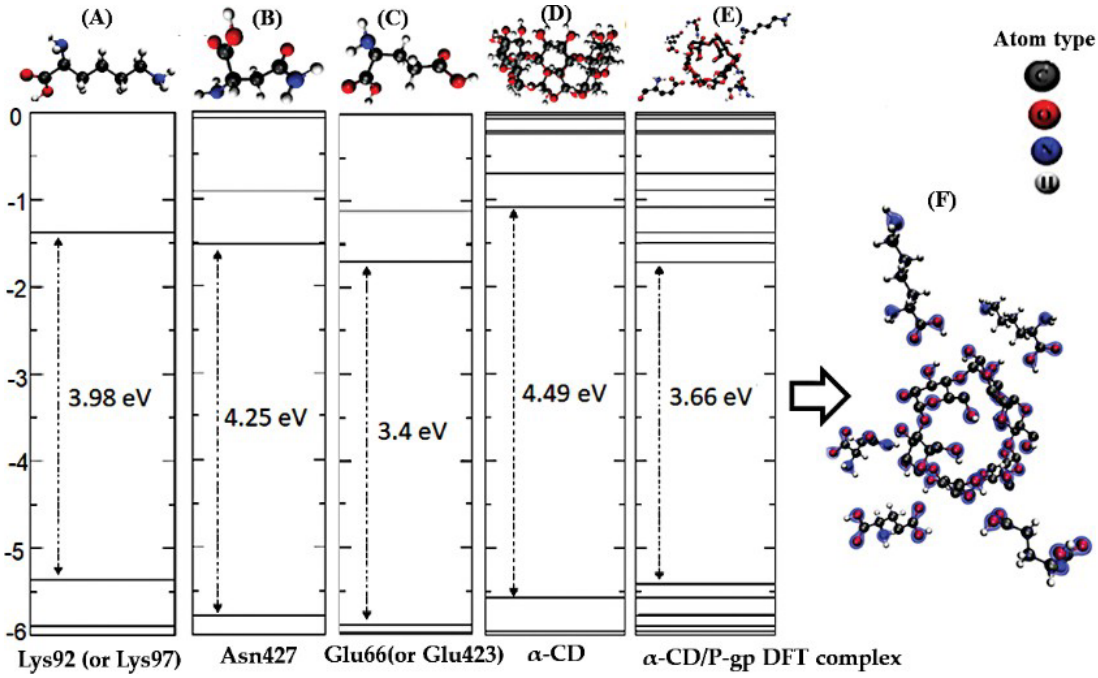


**Fig. (9).** Representation of the electronic levels for the isolated components like **(A)** Lys92 (or Lys97), **(B)** Asn427, **(C)** Glu66(or Glu423), **(D)** α-CD, and the DFT system interacting together as **(E)** α-CD plus P-gp. Lastly, and **(F)** represents the total charge density isosurface, for the final DFT complex obtained as α-CD plus P-gp-target residues by using an orbital charge density isosurfaces of 0.0028 e-/(Å)$^3$. (*A higher resolution / colour version of this figure is available in the electronic copy of the article*).

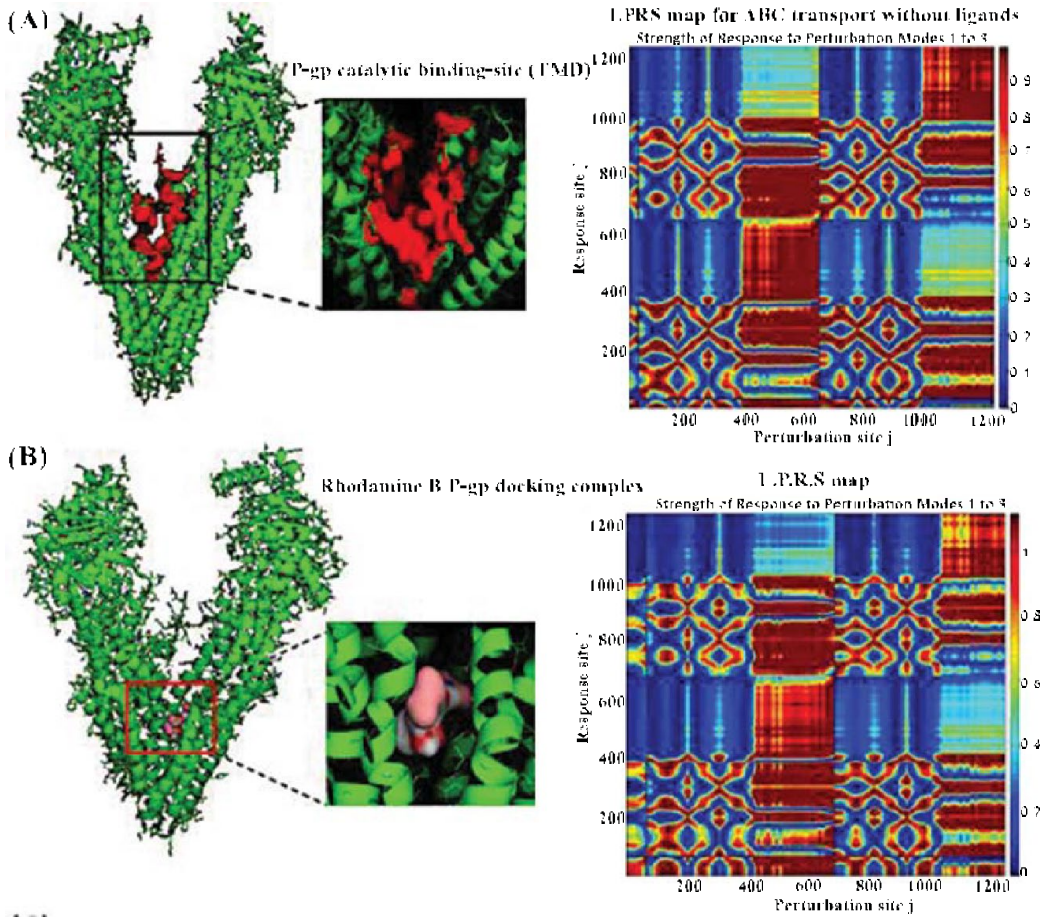


**Fig. (10) contd…**

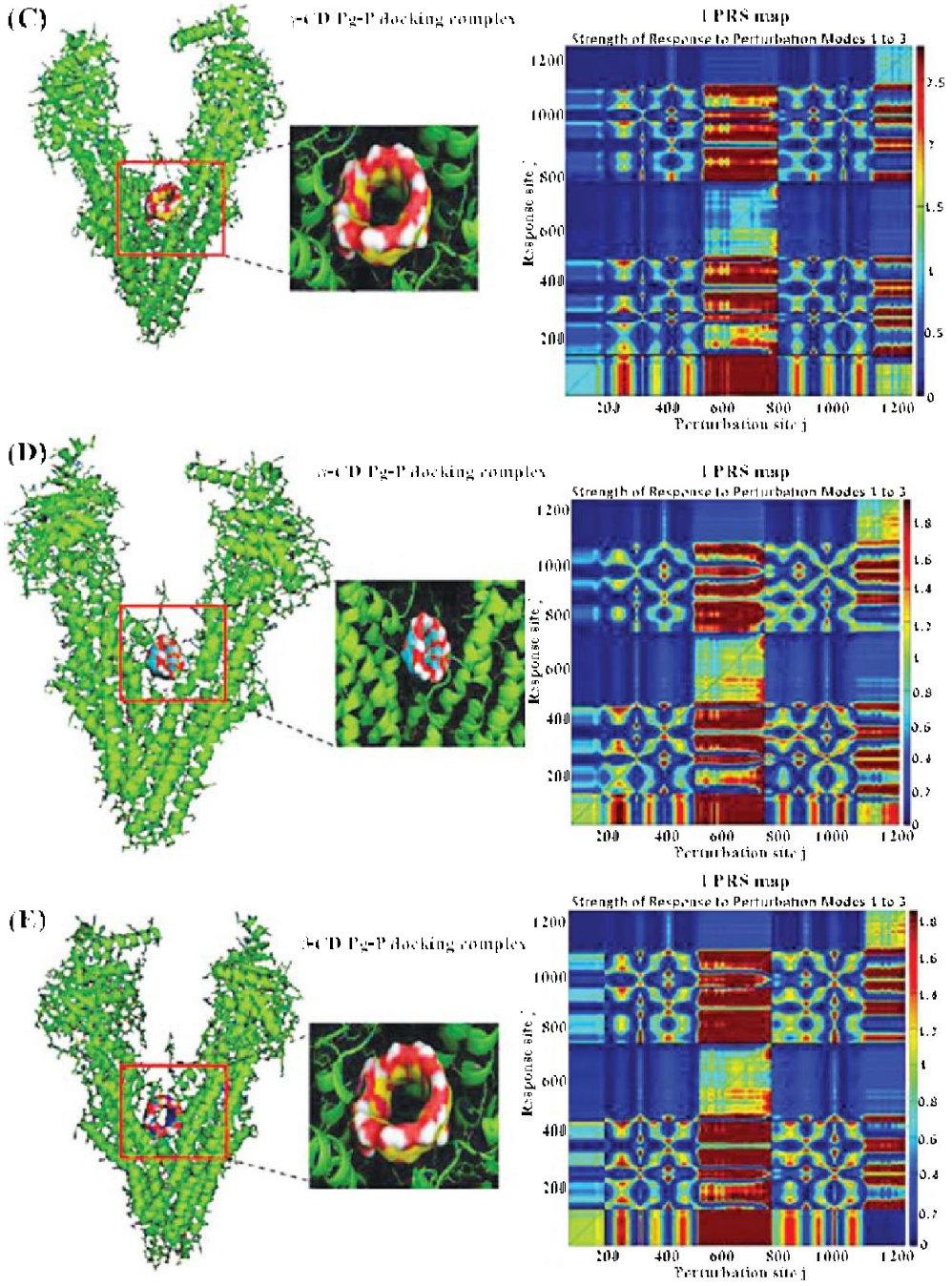


**Fig. (10).** Representation of the 3D-molecular structure of the evaluated protein-ligand complexes with the corresponding LPRS map on the right-site like **(A)** Unperturbed P-gp binding-site (TMD region), **(B)** Rhodamine B/ P-gp as specific P-gp-TMD inhibitor used as control of the simulation, **(C)** γ-CD/ P-gp, **(D)** α-CD/ P-gp/TMDs, and **(E)** β-CD/P-gp/TMDs. For this instance, the range of low-frequency normal modes from 1 to 3 was selected according to collectivity degree, which is highly associated to the collective intrinsic dynamics, local allosteric cooperativity in the P-gp structure, and biochemical functions of P-gp protein on ligand-extrusion. (*A higher resolution / colour version of this figure is available in the electronic copy of the article*).

ligands (*i.e.*, γ-CD, α-CD, and β-CD). Herein, the local perturbations induced by the CD ligands in the residues network of P-gp (C(α)- nodes) were evaluated based on the $e_{p(i)}$ parameter, which represents the effect of the perturbation response in the P-gp (Please refer to equation 3).

For this instance, the row and column of the LPRS maps describe the effectiveness and sensitivity profiles for unperturbed and perturbed P-gp residues in the unoccupied P-gp TMD binding (Fig. **10A**), or presence of ligands (α-CD, β-CD and γ-CD). Specifically, we can see the local perturbations induced by the CD ligands in the residue network by observing the changes in the flexibility of the P-gp TMD binding residues blocks in the LPRS maps where blue regions indicate conformational chain rigidification of the P-gp (*i.e.*, the P-gp target chain A); while orange-to-dark red region indicates conformational chain flexibilization, when

we compare the unbound state (unperturbed residue network) with the bound state in the presence of the CD ligands studied. Herein, the local perturbations were mainly observed in the block of residues located from 1 to 450 residue numbers in the P-gp/TMD binding site in all the LPRS maps obtained.

It is important to note that all the LPRS maps were obtained in the range of low-frequency normal modes which are highly associated with the collective intrinsic dynamics of the P-gp/TMD regions, allosteric cooperativity in the whole P-gp structure and the process of ligand-extrusion of the P-gp protein.

These theoretical observations have a great relevance from the pharmaco-toxicological point of view, considering that this region corresponds to the extrusion-binding domain (as TMDs of P-gp) responsible for the main function of P-gp protein in the blood-brain-barrier (BBB), to avoid potential neurotoxicity effects and events of multi-drug resistance observed in cancer chemotherapy.

## CONCLUSION

In the present study, molecular docking approaches and DFT-ab initio simulations were combined for the first time, to study relevant binding interactions of a cyclodextrin family (α-CD, β-CD and γ-CD) with the multi-drug resistance P-gp protein, toward efficient drug-delivery applications. Then, results of crystallographic validation-based using Ramachandram plots show that all the modeled residues belonging to the P-gp.pdb x-ray structure were conformationally favored showing a total absence of disallowed conformations for interacting P-gp target residues, ensuring the quality of our modeling results. In this regard, the theoretical results point that, despite the differences in the docking interaction patterns for the CDs evaluated, all the cyclodextrins exhibit a very similar affinity-based Gibbs free binding energy. Overall results suggest that the docking-mechanism of the CDs evaluated are mainly based on hybrid backbone/side-chain hydrophobic interactions, and also with the presence of hybrid electrostatic/ backbone/side-chain interactions from the OH-moieties of the CD-ligands and involving electrostatics acceptor and donor interactions. Besides, the results obtained on the local perturbations maps strongly suggest that the CD-ligands can induce significant changes associated with allosteric signals propagation in the inter-residues network of the TMD regions of the P-gp which theoretically could modulate the biochemical function of the P-gp from the pharmacological point of view (CDs-ligand extrusion) during the treatment of neurological disorders or cancer therapy.

Finally, these *in silico* results open new horizons for the evaluation of new nano-therapeutic systems-based cyclodextrins with potential pharmacological relevance for efficient drug-delivery applications; and could promote at the same time, cutting-edge studies in computational neuroscience and precision oncology from a perspective of rational-drug design by using nanotechnology.

## AUTHORS' CONTRIBUTION

Conceptualization and writing-original draft preparation, M.G.-D., L.O.V., I.Z., and M.O.M., methodology-based on Ab initio DFT simulations, L.O.V., I.Z. and M.O.M, methodology-based on molecular docking simulations and local perturbation response maps (LPRS maps), computational crystallographic validation-based Ramachandran diagrams of P-gp protein, M.G.-D., J.M.R. and M.N.D.S.C.; writing-review and editing, M.G.-D., I.Z., R.C., J.M.R., and M.N.D.S.C.; supervision and writing-review and editing, I.Z., J.M.R., and M.N.D.C. All authors have read and agreed to the published version of the manuscript.

## ETHICS APPROVAL AND CONSENT TO PARTICIPATE

Not applicable.

## HUMAN AND ANIMAL RIGHTS

No animals/humans were used for studies that are basis of this research.

## CONSENT FOR PUBLICATION

Not applicable.

## AVAILABILITY OF DATA AND MATERIALS

The data which support the results of this study are available from the corresponding authors (M.G.-D), (R.C); and (M.N.D.S.C.) under request.


## FUNDING

This research was funded by FCT/MCTES through national funds (Michael González-Durruthy, Riccardo Concu, and M. Natália D.S. Cordeiro), grant UID/QUI/50006/2020, as well as by Xunta de Galicia (Juan M. Ruso), grant ED41E2018/08.


## CONFLICT OF INTEREST

Dr. Concu is the Editorial board member of the journal Current Topics in Medicinal Chemistry.


## ACKNOWLEDGEMENTS

The authors M.G-D, R.C, and M.N.D.S.C acknowledge the support from FCT/MCTES through national funds grant UID/QUI/50006/2020. J.M.R acknowledges the support from Xunta de Galicia grant ED41E2018/08. Besides, the authors L.O.V.; I.Z.; and M.O-M acknowledge CENAPAD-SP for the computer time, National Institute of Carbon Nanomaterials-INCT/CNPq; Fapergs, CAPES, and UFN for the financial support.


## REFERENCES


[1] DeGorter, M.K.; Xia, C.Q.; Yang, J.J.; Kim, R.B. Drug transporters in drug efficacy and toxicity. *Annu. Rev. Pharmacol. Toxicol.,* **2012**, *52*(1), 249-273.

http://dx.doi.org/10.1146/annurev-pharmtox-010611-134529 PMID: 21942630

[2] He, Q.; Liu, J.; Liang, J.; Liu, X.; Li, W.; Liu, Z.; Ding, Z.; Tuo, D. Towards improvements for penetrating the blood-brain barrier-recent progress from a material and pharmaceutical perspective. *Cells,* **2018**, *7*(4), 24. http://dx.doi.org/10.3390/cells7040024 PMID: 29570659

[3] Holohan, C.; Van Schaeybroeck, S.; Longley, D.B.; Johnston, P.G. Cancer drug resistance: An evolving paradigm. *Nat. Rev. Cancer,* **2013**, *13*(10), 714-726. http://dx.doi.org/10.1038/nrc3599 PMID: 24060863

[4] De Lange, E.C.M.; Vd Berg, D.J.; Bellanti, F.; Voskuyl, R.A.; Syvänen, S. P-glycoprotein protein expression *versus* functionality at the blood-brain barrier using immunohistochemistry, microdialysis and mathematical modeling. *Eur. J. Pharm. Sci.,* **2018**, *124*, 61-70. http://dx.doi.org/10.1016/j.ejps.2018.08.022 PMID: 30144528

[5] Wu, J.; Lin, N.; Li, F.; Zhang, G.; He, S.; Zhu, Y.; Ou, R.; Li, N.; Liu, S.; Feng, L.; Liu, L.; Liu, Z.; Lu, L. Induction of P-glycoprotein expression and activity by Aconitum alkaloids: Implication for clinical drug-drug interactions. *Sci. Rep.,* **2016**, *6*(1), 25343. http://dx.doi.org/10.1038/srep25343 PMID: 27139035

[6] Kim, N.; Shin, J.; No, K.T. *In silico* study on the interaction between pglycoprotein and its inhibitors at the drug binding pocket. *Bull. Korean Chem. Soc.,* **2014**, *35*(8), 2317-2325. http://dx.doi.org/10.5012/bkcs.2014.35.8.2317

[7] Wongrattanakamon, P.; Lee, V.S.; Nimmanpipug, P.; Sirithunyalug, B.; Chansakaow, S.; Jiranusornkul, S. Insight into the molecular mechanism of P-glycoprotein mediated drug toxicity induced by bioflavonoids: An integrated computational approach. *Toxicol. Mech. Methods,* **2017**, *27*(4), 253-271. http://dx.doi.org/10.1080/15376516.2016.1273428 PMID: 27996361

[8] Zhou, S.F. Structure, function and regulation of P-glycoprotein and its clinical relevance in drug disposition. *Xenobiotica,* **2008**, *38*(7-8), 802-832. http://dx.doi.org/10.1080/00498250701867889 PMID: 18668431

[9] Salim, S. Oxidative stress and the central nervous system. *J. Pharmacol. Exp. Ther.,* **2017**, *360*, 201-205. http://dx.doi.org/10.1124/jpet.116.237503

[10] Montesinos, R.N.; Moulari, B.; Gromand, J.; Beduneau, A.; Lamprecht, A.; Pellequer, Y. Coadministration of P-glycoprotein modulators on loperamide pharmacokinetics and brain distribution. *Drug Metab. Dispos.,* **2014**, *42*(4), 700-706. http://dx.doi.org/10.1124/dmd.113.055566 PMID: 24398461

[11] Ambudkar, S.V.; Dey, S.; Hrycyna, C.A.; Ramachandra, M.; Pastan, I.; Gottesman, M.M. Biochemical, cellular, and pharmacological aspects of the multidrug transporter. *Annu. Rev. Pharmacol. Toxicol.,* **1999**, *39*(1), 361-398. http://dx.doi.org/10.1146/annurev.pharmtox.39.1.361 PMID: 10331089

[12] Muthusamy, G.; Balupillai, A.; Ramasamy, K.; Shanmugam, M.; Gunaseelan, S.; Mary, B.; Prasad, N.R. Ferulic acid reverses ABCB1-mediated paclitaxel resistance in MDR cell lines. *Eur. J. Pharmacol.,* **2016**, *786*, 194-203. http://dx.doi.org/10.1016/j.ejphar.2016.05.023 PMID: 27262378

[13] Han, Y.; Chin Tan, T.M.; Lim, L.Y. *In vitro* and *in vivo* evaluation of the effects of piperine on P-gp function and expression. *Toxicol. Appl. Pharmacol.,* **2008**, *230*(3), 283-289. http://dx.doi.org/10.1016/j.taap.2008.02.026 PMID: 18417181

[14] Silva, R.; Vilas-Boas, V.; Carmo, H.; Dinis-Oliveira, R.J.; Carvalho, F.; de Lourdes Bastos, M.; Remião, F. Modulation of P-glycoprotein efflux pump: Induction and activation as a therapeutic strategy. *Pharmacol. Ther.,* **2015**, *149*, 1-123. http://dx.doi.org/10.1016/j.pharmthera.2014.11.013 PMID: 25435018

[15] Ramos, P.; Schmitz, M.; Gama, S.; Portantiolo, A.; Durruthy, M.G.; de Souza Votto, A.P.; Cornetet, L.R.; Dos Santos Machado, K.; Werhli, A.; Tonel, M.Z.; Fagan, S.B.; Yunes, J.S.; Monserrat, J.M. Cytoprotection of lipoic acid against toxicity induced by saxitoxin in hippocampal cell line HT-22 through *in silico* modeling and *in vitro* assays. *Pharmacol. Ther.,* **2018**, *393*, 171-184. http://dx.doi.org/10.1016/j.tox.2017.11.004 PMID: 29128272

[16] Marques, M.B.; de Oliveira, P.V.; Fagan, S.B.; Oliveira, B.R.; da Silva Nornberg, B.F.; Almeida, D.V.; Marins, L.F.; González-Durruthy, M. Modeling drug-drug interactions of AZD1208 with Vincristine and Daunorubicin on ligand-extrusion binding TMD-domains of multidrug resistance P-glycoprotein (ABCB1). *Toxicology,* **2019**, *411*, 81-92. http://dx.doi.org/10.1016/j.tox.2018.10.009 PMID: 30339824

[17] Trott, O.; Olson, A.J. AutoDock Vina: Improving the speed and accuracy of docking with a new scoring function, efficient optimization, and multithreading. *J. Comput. Chem.,* **2010**, *31*(2), 455-461. PMID: 19499576

[18] Kelley, L.A.; Mezulis, S.; Yates, C.M.; Wass, M.N.; Sternberg, M.J. The Phyre2 web portal for protein modeling, prediction and analysis. *Nat. Protoc.,* **2015**, *10*(6), 845-858. http://dx.doi.org/10.1038/nprot.2015.053 PMID: 25950237

[19] Forli, S.; Huey, R.; Pique, M.E.; Sanner, M.F.; Goodsell, D.S.; Olson, A.J. Computational protein-ligand docking and virtual drug screening with the AutoDock suite. *Nat. Protoc.,* **2016**, *11*(5), 905-919. http://dx.doi.org/10.1038/nprot.2016.051 PMID: 27077332

[20] Berman, H.M.; Westbrook, J.; Feng, Z.; Gilliland, G.; Bhat, T.N.; Weissig, H.; Shindyalov, I.N.; Bourne, P.E. The protein data bank. *Nucleic Acids Res.,* **2000**, *28*(1), 235-242. http://dx.doi.org/10.1093/nar/28.1.235 PMID: 10592235

[21] Tao, A.; Huang, Y.; Shinohara, Y.; Caylor, M.L.; Pashikanti, S.; Xu, D. ezCADD: A rapid 2D/3D visualization-enabled web modeling environment for democratizing computer-aided drug design. *J. Chem. Inf. Model.,* **2019**, *59*(1), 18-24. http://dx.doi.org/10.1021/acs.jcim.8b00633 PMID: 30403855

[22] Xie, Z.R.; Hwang, M.J. An interaction-motif-based scoring function for protein-ligand docking. *BMC Bioinformatics,* **2010**, *11*(1), 298. http://dx.doi.org/10.1186/1471-2105-11-298 PMID: 20525216

[23] Mitternacht, S.; Berezovsky, I.N. Coherent conformational degrees of freedom as a structural basis for allosteric communication. *PLOS Comput. Biol.,* **2011**, *7*(12), e1002301. http://dx.doi.org/10.1371/journal.pcbi.1002301 PMID: 22174669

[24] Keskin, O.; Durell, S.R.; Bahar, I.; Jernigan, R.L.; Covell, D.G. Relating molecular flexibility to function: A case study of tubulin. *Biophys. J.,* **2002**, *83*(2), 663-680. http://dx.doi.org/10.1016/S0006-3495(02)75199-0 PMID: 12124255

[25] Greener, J.G.; Sternberg, M.J. AlloPred: Prediction of allosteric pockets on proteins using normal mode perturbation analysis. *BMC Bioinformatics,* **2015**, *16*(1), 335. http://dx.doi.org/10.1186/s12859-015-0771-1 PMID: 26493317

[26] Hohenberg, P.; Kohn, W. Inhomogeneous electron gas. *Phys. Rev.,* **1964**, *136*(3B), 864-871. http://dx.doi.org/10.1103/PhysRev.136.B864

[27] Kohn, W.; Sham, L.J. Self-consistent equations including exchange and correlation effects. *Phys. Rev.,* **1965**, *140*(4A), 1133-1138. http://dx.doi.org/10.1103/PhysRev.140.A1133

[28] Soler, J.M.; Artacho, E.; Gale, J.D.; García, A.; Junquera, J.; Ordejón, P.; Sánchez-Portal, D. The SIESTA method for ab-initio order-N materials simulation. *J. Phys. Condens. Matter,* **2002**, *14*(11), 2745-2779. http://dx.doi.org/10.1088/0953-8984/14/11/302

[29] Troullier, N.; Martins, J.L. Efficient pseudopotentials for plane-wave calculations. *Phys. Rev. B Condens. Matter,* **1991**, *43*(3), 1993-2006. http://dx.doi.org/10.1103/PhysRevB.43.1993 PMID: 9997467

[30] Perdew, J.P.; Burke, K.; Ernzerhof, M. Generalized gradient approximation made simple. *Phys. Rev. Lett.,* **1996**, *77*(18), 3865-3868. http://dx.doi.org/10.1103/PhysRevLett.77.3865 PMID: 10062328

[31] González-Durruthy, M.; Concu, R.; Vendrame, L.F.O.; Zanella, I.; Ruso, J.M.; Cordeiro, M.N.D.S. Targeting beta-blocker drug-drug interactions with fibrinogen blood plasma protein: A computational and experimental study. *Molecules,* **2020**, *25*(22), 5425. http://dx.doi.org/10.3390/molecules25225425 PMID: 33228181

[32] Boys, S.F.; Bernardi, F. The calculation of small molecular interactions by the differences of separate total energies. Some procedures with reduced errors. *Mol. Phys.,* **1970**, *19*(4), 553-566. http://dx.doi.org/10.1080/00268977000101561

[33] Oviedo, M.B.; Wong, B.M. Real-time quantum dynamics reveals complex, many-body interactions in solvated nanodroplets. *J. Chem. Theory Comput.,* **2016**, *12*(4), 1862-1871. http://dx.doi.org/10.1021/acs.jctc.5b01019 PMID: 26918732

[34] Vendrame, L.; Schimtz, B.; Fagan S.; Zanella, I. Ciclodextrines interacting with methotrexate *via* molecular modeling. *Disciplinarum Sci., Série: Naturais e Tecnológicas*., **2018**, *19*(3), 401-412.

[35] Jiménez, J.; Doerr, S.; Martínez-Rosell, G.; Rose, A.S.; De Fabritiis, G. DeepSite: Protein-binding site predictor using 3D-convolutional neural networks. *Bioinformatics,* **2017**, *33*(19), 3036-3042. http://dx.doi.org/10.1093/bioinformatics/btx350 PMID: 28575181

[36] Chen, V.B.; Arendall, W.B., III; Headd, J.J.; Keedy, D.A.; Immormino, R.M.; Kapral, G.J.; Murray, L.W.; Richardson, J.S.; Richardson, D.C. MolProbity: All-atom structure validation for macromolecular crystallography. *Acta Crystallogr. D Biol. Crystallogr.,* **2010**, *66*(Pt 1), 12-21. http://dx.doi.org/10.1107/S0907444909042073 PMID: 20057044

[37] González-Durruthy, M.; Werhli, A.V.; Seus, V.; Machado, K.S.; Pazos, A.; Munteanu, C.R.; González-Díaz, H.; Monserrat, J.M. Decrypting strong and weak single-walled carbon nanotubes interactions with mitochondrial voltage-dependent anion channels using molecular docking and perturbation theory. *Sci. Rep.,* **2017**, *7*(1), 13271. http://dx.doi.org/10.1038/s41598-017-13691-8 PMID: 29038520

[38] Bartosiewicz, D.; Krasowska, A. Inhibitors of ABC transporters and biophysical methods to study their activity. *Z. Naturforsch. C J. Biosci.,* **2009**, *64*(5-6), 454-458. http://dx.doi.org/10.1515/znc-2009-5-625 PMID: 19678554